PCCP

The Competitive Strengths of Hydrogen and Halogen Bonding to Haloforms and Their Different Spectroscopic Markers

Journal:	*Physical Chemistry Chemical Physics*
Manuscript ID	CP-ART-01-2025-000059.R1
Article Type:	Paper
Date Submitted by the Author:	22-Feb-2025
Complete List of Authors:	Scheiner, Steve; Utah State University, Department of Chemistry and Biochemistry

The Competitive Strengths of Hydrogen and Halogen Bonding to Haloforms and Their Different Spectroscopic Markers

Steve Scheiner*

Department of Chemistry and Biochemistry
Utah State University
Logan, Utah 84322-0300
USA

*email: steve.scheiner@usu.edu

Abstract

Haloforms (CX_3H) are paired with halide anions and with neutral N-bases, and the properties of the ensuing hydrogen (HB) and halogen bond (XB) are examined by DFT calculations. The strength of either sort of interaction diminishes in the order $F^- > Cl^- > Br^- > I^- > NH_3 > NCH$. The XB energy climbs rapidly as the haloform X atom grows larger, but the HB is much less sensitive to the identity of X. In most cases, the HB is energetically favored over the XB. Exceptions occur when CI_3H is paired with any of the halides, where the XB is more stable. In both cases, the X-H stretching frequency is shifted to the red, but the magnitude of this shift is far larger in the HB case. The NMR chemical shielding of the proton is substantially reduced by formation of a HB, but undergoes a small increase within the XB. The C nucleus of the haloform suffers a large shielding drop within the HB, but its shielding change is far smaller within the context of a XB, and can be of either sign.

Keywords: σ-hole; red shift; vibrational frequency; NMR shielding

INTRODUCTION

The prevalence and importance of the H-bond (HB) has motivated intense scrutiny over the last century. This noncovalent interaction is a major player in solvation and the structure and function of a wide range of biological systems [1-7]. The HB is partly responsible for the stability of proteins and the mechanism of numerous enzymes. A key means of probing this phenomenon is spectroscopy. One can take as a quantitative measure of the strength of each such bond the degree of shift and intensification that occurs in certain IR bands; an alternate metric is associated with the displacement of various NMR peaks [8-10]. The Badger-Bauer rule relates the strength of a given HB to the red shift observed in the covalent A-H stretching frequency of the proton donor [11-13], NMR spectroscopy offers a similar window, using the downfield shift of the NMR peak of the bridging proton as its key parameter.

The last few decades have reawakened interest in a set of noncovalent bonds that bear a striking resemblance to the HB. In each, the HB proton bridge is replaced by a larger atom, many but not all more electronegative than H. The overall partial charge of the original H occurs instead as a σ-hole, a smaller positive region, surrounded by a negative belt. Depending upon the family of elements from which this replacement atom is drawn, each such σ-hole bond is commonly categorized as a halogen, chalcogen, pnicogen bond and so forth. But the basics of the HB remain: these noncovalent interactions derive their strength from a mixture of electrostatic, polarization, charge transfer, and dispersion [14-28]. Also in common with the HB, each σ-hole bond is strengthened by electron-withdrawing substituents on the Lewis acid which intensify this hole. Another factor which enters into the equation is the row of the periodic table. The increasing polarizability and diminishing electronegativity enhances the bond as the bridging atom moves down further in the periodic table, as for example the Cl < Br < I sequence for halogen bonds. First-row atoms, i.e. F, O, N, and C, engage in only weak bonds of this type if at all, but can be coaxed into measurable interactions by appropriate substituents or adding a charge [29-33].

Of this family of noncovalent interactions, it is the halogen bond (XB) that has accunulated the longest and most substantive record of research. Its acute similarity to the HB in a number of respects raises the question as to which of these two bonds is the stronger. An obvious means by which to address this issue experimentally is via spectroscopy. As indicated above, the features derived from both IR and NMR spectra have provided a convenient gauge of HB strength, which leads to the question as to their applicability to the parallel XBs. Previous studies of the NMR spectroscopy of halogen-bonded complexes [34-42] have offered insights into the nature of this sort of bonding. For example, it was found that the coupling constant of the base can serve as a gauge of both the geometry and strength of the XB [43]. ^{13}C NMR measurements verified a charge transfer from iodide ions to HCI_3 molecules.

Computational studies have supplemented experimental work with additional findings from another perspective [44-48]. Interpretation of the ^{13}C signal of the C bonded to I in iodoalkynes [49] led to the conclusion that its downfield shift arises from polarization of the triple bond. Calculated data [50] of 27 pyridine oxides were able to point to the most important contributors to

their halogen bonding. The importance of secondary interactions to the NMR spectra of (imide)N–X···N(pyridine) halogen-bonded complexes was elucidated [48]. The correlation between the coupling constants and the corresponding bond lengths enable added insights as to the nature of these bonds [51].

Regarding the central question as to the competition between a HB and XB, there have been several relevant studies encompassing a range of different molecules [52-59]. The haloform CX_3H set of molecules offers an ideal forum by which to answer this question, as it contains both the H and X atoms on the same molecule, and even bonded to the same C atom. The molecule is also small enough so as to avoid complicating effects from more distant groups. This haloform series has in fact engendered some past study [40, 60-64]. The prior work had found that the relative stabilities of the two types of bonding scenarios seemed to depend on several factors. The nature of the X atom was important, as was the type of nucleophile which participated in the bonding, and there was some dependence also on the particular solvent in which the measurements were made.

The current work is designed to first provide a more definitive exploration of the nature of the HB and XB to the haloforms, and to elucidate which of these two bond types is energetically preferred and why. This question is addressed via quantum chemical calculations directed at a set of systems that are both accessible to experiment, and diverse enough to cover a range of bond strengths. Each of the four CX_3I haloforms (X=F, Cl, Br, I) are paired with a set of nucleophiles of both neutral and anionic type. All four halides are included in this list of nucleophiles, ranging from F^- to I^-, as are two N-bases: The sp^3 hybridization of NH_3 makes for a strong neutral nucleophile, while the sp hybridization of NCH borders on the weakest limits. Altogether, this set of bases covers a wide range of strength. In order to facilitate communication with experimentally accessible measurements, the IR and NMR spectra of these complexes are calculated and analyzed. The work is designed also to provide diagnostics as to how to interpret these spectra so as to determine which of the two bonds might be present, and how strong it might be.

METHODS

The Gaussian 16 package [65] was applied to perform the quantum chemical calculations of the systems described below. These calculations employed the DFT approach and in particular the M06-2X functional [66-68], within the framework of the def2-TZVP basis set. M06-2X has been repeatedly assessed to be one of the most accurate functionals for noncovalent interactions [69-77]. The lack of imaginary harmonic frequencies affirmed the structures as true minima. Interaction energies were derived as the difference in total energy between the complex on one hand, and the sum of subunit energies on the other, each computed in the geometry they adopt within the dyad. This quantity was corrected for basis set superposition error with the aid of the Boys-Bernardi counterpoise procedure [78]. The MEP (molecular electrostatic potential) was analyzed so as to locate and quantify the maxima for each subunit on the 0.001 au electronic isodensity contour, utilizing the MultiWFN software [79, 80]. Using the AIMAll program [81], the QTAIM topological

analysis [82, 83] of the electron density added information about interactions between atoms, represented by bond paths and their bond critical points. Estimation of NMR parameters employed the Gauge-Invariant Atomic Orbital [84, 85] scheme.

RESULTS

Monomer Properties

An important property of each CX_3H monomer is the molecular electrostatic potential (MEP) that surrounds it, particularly close to the X and H centers which attract the nucleophile. This MEP is diagrammed for each of the haloform molecules in Fig 1. The positive blue region is clearly most intense near the H atom, with a weaker σ-hole appearing along the extension of each C-X bond axis. This hole intensifies as the X atom grows larger. One can distill this potential as the maximum in the MEP that occurs near to the X and H atoms, which is evaluated on the 0.001 au isodensity surface. This quantity, labeled as V_{max}, is presented for each haloform molecule in Table 1. This maximum value is considerably larger for the H than for X, although this difference drops as the X atom grows larger and less electronegative, consistent with Fig 1. In fact, there is no maximum on the 0.001 au density surface for F. It is also worth stressing that the maximum on the X atom rises dramatically with X size, but there is a much more gradual change in the opposite direction for V_{max} on H.

Geometries

The general dispositions of the two molecules relative to one another are described in Fig 2 for several exemplary dyads. The upper diagrams refer to the H-bonded structures, while the halogen-bonded conformers are presented in the bottom. The intermolecular distance R is defined as that between the H or X atom, respectively, and the halide or N center of the incoming nucleophile. Any nonlinearity around the H and X atoms is represented by the α angle.

Table 2 lists the R and α parameters in the various optimized dyads. It should be noted first that the high electronegativity of F, and its inability to encompass a σ-hole, prevents the formation of fluoroform to engage in halogen-bonded complexes with any of the bases. As a second issue, the very high proton-attracting power of the F^- anion leads to a proton transfer (pT) to it from any of the haloforms other than CF_3H, leading instead to a CX_3^- + HF pair, so no H-bonded geometries are listed.

There are several relevant patterns that are evident in Table 2. Focusing first on the angles α, most of the geometries are very close to linear, whether CH··X/N or CX··X/N. The major exceptions occur for the H-bonded dimers pairing the two neutral bases with the heavier haloforms. The reasons for these nonlinearities are discussed in some detail below. With regard to the HB distances, these elongate along with the enlarging of the halide: $F^- < Cl^- < Br^- < I^-$. Also, this length is shorter for NH_3 than for NCH, along with the stronger nucleophilicity of the former and its sp^3 hybridization as compared to sp for the latter. For any given base, the HB length contracts as the X atom within CX_3H grows larger. The intermolecular distances are of course longer for the XB than HB dyads, since the X atom is so much larger than H. And these distances within the XB subset grow longer for heavier X^- anions for the same reason. But for any given halide, there is a tendency for R to shorten as the X within the haloform grows heavier, despite the larger atomic radii, as well as longer distances for NCH as compared to NH_3.

Energetics

The strength of the HB and XB binding is assessed as the interaction energy between the two subunits within each dyad. These quantities are contained within the first two columns of Table 3, and exhibit some interesting patterns. Both the HB and XB strengths clearly drop as the halide becomes larger with lower charge concentration. Also these bonds are stronger for the halides than for the two neutral bases, a clear example of "charge assistance". Perhaps more interesting is the effect of the X atom of the haloform on the two bond types. The HB energy grows, but only very slowly, as X grows larger. The XB also grows stronger by this transformation but far more dramatically.

These patterns are more easily visualized in Fig 3 where the blue and red curves correspond to the HB and XB, respectively. For each nucleophile, both the blue and red curves rise to the right, with a much stronger rise in the red XB curve. One can also see the drop from left to right as each nucleophile gets weaker: $F^- > Cl^- > Br^- > I^- > NH_3 >$ NCH. There is consistency between the energetics and bond lengths in Table 2. The strengthening of each HB is accompanied by its shortening. The same is true of the XBs, but one must also bring the larger radius of the heavier X atoms into the equation. It is also intriguing to note where the red and blue curves intersect and cross one another. In most cases, the HB is stronger for all of the haloforms with the exception of CI_3H, for which the XB exceeds the HB.

The complexation of the two subunits leads to geometrical perturbations within each. The most important of these is the change in the C-H bond length within the haloform. The next two columns of Table 3 report these changes for both the HB and XB type complexes. While both sorts of bonds cause an elongation of the CH bond, these stretches are far larger within the context of the HBs. Some of these elongations parallel the energetics. The stretches are largest for Cl^-, and are reduced as the halide is enlarged up to I^-, and then further lowered for NH_3 and then NCH. For a given Lewis base, the stretches are smallest for fluoroform, and progressively larger for Cl, Br, and then I. The stretches in r(CH) engendered by the XBs are quite small and do not obey a universal pattern. On the other hand, the elongations are consistently largest for the F^- Lewis base.

Vibrational Spectra

The succeeding two columns of Table 3 present the change introduced into the CH stretching frequency of each haloform by its complexation with the indicated Lewis base. In most cases, there is a red shift, indicated by a negative value of $\Delta\nu$, consistent with the prior observation that these CH bonds elongate. These shifts are far more dramatic for the HB than for the XB, again in line with the much longer stretches of the former. This distinction is sensible in light of the direct interaction of the base with the CH bond in the former sort of bonding. The red shift is notable in light of the blue shifting of a CH stretch that frequently accompanies sp^3 hybridization of the C atom in related HBs [86-88]. There is some consistency with the CH bond stretches in that longer stretches correspond to larger red shfits.

Fig 4 presents the patterns in these frequency shifts where the much more negative values for the HBs of the blue curve are in clear evidence. The red shift grows along with the size of the X atom within the haloform. As well, the red shifts are most intense for the smaller halides $Cl^- > Br^- > I^-$; these shifts are smaller still for the neutral bases. The F systems are again an exception, as CF_3H forms a HB only with F^-. That bond is exceedingly short and strong, with R(H··F) only 1.4 Å and with an interaction energy of 36.9 kcal/mol.

In common with the vast majority of HBs, the intensity of the CH stretching mode is enhanced by the HB formation. These increases are displayed in the final two columns of Table 3 as the ratio between the intensity in the complex versus that within the haloform monomer. This ratio can be quite large, more than 1000 in two cases. There is a clear pattern that the ratio is largest for Cl^- and drops quickly as the anion grows in size, and then even smaller for the two neutral bases. This ratio also drops precipitously as the X atom within the haloform changes from Cl to Br and then to I. As in many of the other features, F again represents an exception. The intensification of the CH stretching mode is much smaller in fluoroform, even dropping below unity for the two neutral bases. The effect of the XB upon the CH intensity is far smaller, even diminishing it in quite a number of cases.

Overall, then, the IR spectra furnishes a clear division between the presence of a HB or XB. The CH stretching frequency undergoes a very substantial red shift for the HBs, along with a large intensification of the spectroscopic band. It also shifts to the red when the haloform is involved in a XB, but this shift is an order of magnitude smaller. Another clear distinction is the large intensification of the CH stretching band, which is absent in the XB complexes.

NMR Spectra

The chemical shielding about the C and H atoms of the haloform ought to be susceptible to modulation caused by complexation, particularly H-bonding which would directly involve the proton. The effects of each dimerization upon their shielding are displayed in Table 4, where it is first clear that the bridging proton suffers a substantial shielding reduction when the haloform participates in a HB, as much as 10.6 ppm. However, this pattern is reversed to a shielding increase, albeit a small one of less than 1 ppm, if it is a XB that is formed. The deshielding of the H-bonding proton shadows the HB interaction energy to some degree. This deshielding becomes smaller as the halide radius grows larger, and is fairly insensitive to the identity of the X atom within the haloform.

This pattern is visible by inspection of the blue curve in Fig 5 which also illustrates the deshielding is smaller in fluoroform than in the other haloforms for each nucleophile. The small shielding increases of this proton caused by the XBs are plain in the red curves, which also depict how this increase slowly rises as the X atom of CX_3H becomes heavier. (It should perhaps be stressed that a diminished shielding is tantamount to a downfield shift of the NMR signal, and a larger δ quantity.)

The shielding about the C atom is considerably more sensitive to complexation that is that of the H. In most cases, the C suffers a loss of shielding, which can be as large as 33 ppm. This deshielding is sensitive to both the nature of the X within the haloform and the power of the nucleophile. From consideration of the data in Table 4 and its graphic illustration in Fig 6, the heavier X atoms cause a rapid rise in the degree of deshielding, whether HB or XB. This quantity also increases as the nucleophile's potency rises, in the order $F^- > Cl^- > Br^- > I^- > NH_3 >$ NCH. Of particular note, the C deshielding is considerably larger for the HBs than for the XBs. There is also the curious reversal of trends for the neutral bases. In these cases, the shielding of the C atom is increased by XB formation, and this shielding increase rises as the X atom within the haloform grows larger.

With regard to fundamental distinctions between hydrogen and halogen bonding, the former causes a very substantial deshielding of the proton, whereas its shielding increases modestly upon XB formation. With respect to the C nucleus, it is consistently deshielded by the HBs and by a fairly large amount. Halogen bonding causes smaller changes, whose direction depends

upon the nature of the base. C is deshielded by halide anions, but its shielding rises for neutral nucleophiles. In either case, the magnitude of this change is much smaller for XBs than for HBs.

DISCUSSION

Most of the dyad geometries are linear, or nearly so, with α angles close to 180°, as is typically expected for either a HB or XB. The major exceptions occur for the H-bonded structures of the two neutral nucleophiles NH_3 and NCH with the haloforms for X=Cl, Br, and I, where these angles lie between 131° and 149°. A glance at the structures in Fig 2 suggests there may be secondary interactions drawing the H atoms of the two bases down toward the halogen atoms of the haloform. And indeed, there would be a certain degree of coulombic attraction that would stabilize such bending of the HB. AIM bond paths in Figs 7a-7c argue against a formal bonding of that sort for the complexes involving NH_3. NCI diagrams, on the other hand [89], suggest at least a small degree of noncovalent bonding, as evident by the green areas in Figs 8a-8c that supplement the N··H disk. Supplementary bond paths do appear in the AIM diagrams for the NCH complexes, connecting the X atoms of the haloform with the NC bond of NCH in Figs 7d-f. These auxiliary bonds are present also in the NCI diagrams in Figs 8d-8f. This secondary bonding cannot be ignored as their bond critical point densities of 0.006 au are each slightly more than half the 0.010 au of the H··N HB.

A supplementary answer to the question as to what forces pull these HBs out of linearity arises from NBO analysis. Taking the $Cl_3CH··NH_3$ system as an example, NBO finds a second-order perturbation energy E2 of 3.30 kcal/mol due to charge transfer from the N lone pair to the σ*(CH) antibonding orbital of Cl_3CH, typical of HBs in general. The spatial disposition of these two orbitals and their strong overlap is depicted in Fig 9a. But Fig 9b illustrates that the same N lone pair overlaps rather nicely with a second orbital of the Cl_3CH unit. In particular, there is a close coincidence with the σ*(C-Cl) orbital, which is facilitated by the aforementioned bending of the HB away from linearity. The E2 for this interaction is equal to 0.96 kcal/mol, a bit smaller than that for the primary HB interaction, but substantial enough that it encourages this bending. Given the transfer into the σ*(C-Cl) orbital, this secondary interaction might be best characterized as a tetrel bond, albeit one not evident from an AIM molecular diagram. With respect to the halogen-bonded complexes with the neutral nucleophiles, there is no such pull toward nonlinearity due to the strong overlap with the σ*(CX) antibonding orbital when the system is fully linear.

The calculated NMR shielding data are fairly consistent in the prediction that one can expect a significant downfield shift of the haloform proton by several ppm when it is engaged in a HB. If the interaction consists instead of a XB, the signal of this proton will shift in the opposite direction by a smaller amount, on the order of 1 ppm or less. These trends are fully consistent with the prior experimental findings [61] which combined each of the haloforms with halides Cl^-, Br^-, and I^-. The proton was deshielded by between 1 and 3 ppm for most of the haloforms with the exception of CI_3H for which there was a small upfield shift of 0.3 ppm. These trends suggest that it is the HB that is energetically preferred over the XB for all of the haloforms except the latter iodoform. Inspection of the energetics in Table 3 confirms this experimental supposition from a computational perspective. The calculations find that for each of these halide anions, the HB is more stable than the XB for all of the haloforms with the exception of CI_3H, where the XB is preferred by some 6-8 kcal/mol.

With respect to neutral bases, the earlier work [61] had measured downfield proton shifts when each of the haloforms was complexed with pyridine. This finding comports with the calculations

which found preference for the HB over the XB, even for iodoform. It might be noted that the downfield shift for iodoform was smaller than for either chloroform or bromoform. This smaller value might signal an equilibrium between HB and XB geometries, a result which is consistent with the very similar calculated energies of these two conformers when iodoform is paired with NH_3. This near equality of energies remains even if the HB and XB geometries are immersed in CCl_4 solvent, as in the experiment. PCM simulation of this solvent leaves the two conformers within 1 kcal/mol of one another. Also with respect to neutral N-bases, Bertrán et al [90] had later measured downfield shifts of the haloform proton between 1.0 and 1.4 ppm, only slightly lower than the shifts calculated here with NH_3. This shift drops for iodoform, consistent with the predilection of this molecule to engage in halogen instead of hydrogen bonding. These authors noted that these same trends persist for the CX_2H_2 methylene halides, although the shifts are a bit smaller. They also observed perturbations of some of these trends upon variation of solvent [91].

The data reported here are consistent with earlier calculations on related systems. Watson et al [92] had also noted a weak dependence of the HB interaction energies of the haloform series upon the identity of the X atom, whereas the XB energies are much more sensitive to this factor. As observed here, the proton's NMR signal was perturbed much more by hydrogen than by halogen bonding, and in the opposite direction. It is comforting to note the DFT calculations were able to nicely approximate experimental NMR proton shifts, and to closely mimic some of the details of the X-ray structures. Direct comparison of the numerical values with those presented here are complicated since the prior work placed the systems within the confines of a solvent. However, the supplementary information of that paper [92] contained gas phase interaction energies which are quite close to those in Table 3. This particular paper supplemented an earlier work by some of these authors [93] which had documented the presence of both HBs and XBs when CH_3Br was paired with halide anions within the context of a crystal.

Martire et al [62] had measured the ΔH for the H-bonding interactions of $CHCl_3$ and $CHBr_3$ with the N base di-n-octylmethylamine to be 4.2 and 3.8 kcal/mol, respectively. The replacement of this amine by the smaller NH_3 here, with its similar sp^3-hybridized N, yields calculated enthalpies of 4.0 and 4.8 kcal/mol. This level of agreement is quite good, considering the different bases, as well as the experimental measurements being conducted in liquid cyclohexane. Another point of agreement is that the experiments failed to observe halogen bonding, consistent with the computational finding that the HB structure is considerably more stable than XB for these two haloforms. An earlier measurement [60] of the enthalpy of the association between CF_3I and a different N-base, 2,4,6-trimethylpyridine, yielded a value of 5.0 kcal/mol, mimicked nicely by the enthalpy calculated here of 4.8 kcal/mol for its interaction with NH_3.

The preference of a halide for the I atom of iodoform as opposed to its H was confirmed earlier [40] by a crystal diffraction study. This same report noted an increase in the NMR shielding of the iodoform proton, consistent with what was found here for a halogen bond interaction. The measurements noted also a reduced shielding on the C atom, fully consistent with the calculated deshielding when CI_3H is involved in a XB with a halide. Indeed, even the measured magnitude of this deshielding of about 10 ppm falls squarely within the range of computed values between 7 and 11 ppm. Recent experimental measurements of the proton NMR signal in CX_3H [64] confirm the switching from HB for X=Cl and Br to XB for I when the haloform is complexed with a neutral DABCO N-base. Further, the calculated NMR shift changes of the proton were quite consistent with those in Table 4 for NH_3 as base.

CONCLUSIONS

The calculations reported here find that both the H and X atoms of the haloforms can engage in a fairly strong interaction with either halides or neutral N-bases. While the XB energy climbs quickly as the X atom of the CX_3H is enlarged, there is much less sensitivity of the HB to the identity of this atom. When interacting with halides, the HB is energetically favored over the XB configuration for all haloforms save CI_3H where the latter is more stable. The preference for the HB extends to neutral N-bases as well, with the exception of iodoform where the two types of bonding are very nearly equal in energy when paired with NH_3. The HB and XB interactions present different and distinct spectroscopic manifestations. In both cases, the X-H stretching frequency is shifted to the red, but the magnitude of this shift is far larger in the HB case. The NMR chemical shielding of the proton is substantially reduced by formation of a HB, but undergoes a small increase within the XB. The C nucleus of the haloform also presents a tell-tale signal as to bond type. It suffers a large shielding drop within the HB, more than 20 ppm in some cases. Within the context of a XB, on the other hand, the shielding change about the C nucleus is far smaller, and can be of either sign.

These trends can be applied to predict and understand the manner in which the series of haloforms will manifest their interactions with various nucleophiles through spectral measurements. As the X atom grows larger there will be a steady migration away from H-bonding to a halogen-bonded interaction. This transition will lead to a much smaller red shift of the C-H stretching frequency. The NMR chemical shielding on the proton will reverse in sign, from a downfield shift of several ppm to a much smaller, and possibly upfield shift. This same pattern will occur in the ^{13}C signal, with a larger magnitude that can reach more than 10 or even 20 ppm. The specific point of transition from HB to XB will vary, depending upon the strength of the nucleophile. For strong anionic bases, the transition will occur clearly between Br and I, but will be delayed for weaker neutral nucleophiles, for which the HB may be preferred over the entire range of haloforms.

Acknowledgments

This material is based upon work supported by the U.S. National Science Foundation under Grant No. 1954310.

Conflicts of interest

There are no conflicts to declare.

REFERENCES

1. G. C. Pimentel and A. L. McClellan, *The Hydrogen Bond*, Freeman, San Francisco, 1960.
2. D. Hadzi and S. Bratos, in *The Hydrogen Bond. Recent Developments in Theory and Experiments*, eds. P. Schuster, G. Zundel and C. Sandorfy, North-Holland Publishing Co., Amsterdam1976, vol. 2, pp. 565-611.
3. M. D. Joesten and L. J. Schaad, *Hydrogen Bonding*, Marcel Dekker, New York, 1974.
4. G. Gilli and P. Gilli, *The Nature of the Hydrogen Bond*, Oxford University Press, Oxford, UK, 2009.

5. S. Scheiner, *Hydrogen Bonding: A Theoretical Perspective*, Oxford University Press, New York, 1997.
6. S. J. Grabowski, *Understanding Hydrogen Bonds: Theoretical and Experimental Views*, Royal Society of Chemistry, Cambridge, 2021.
7. S. M. Cybulski and S. Scheiner, *J. Am. Chem. Soc.*, 1989, **111**, 23-31.
8. L. A. Rivera-Rivera, B. A. McElmurry, K. W. Scott, R. R. Lucchese and J. W. Bevan, *J. Phys. Chem. A*, 2013, **117**, 8477-8483.
9. J. L. Cook, C. A. Hunter, C. M. R. Low, A. Perez-Velasco and J. G. Vinter, *Angew. Chem., Int. Ed. Engl.*, 2007, **46**, 3706-3708.
10. L. Du, K. Mackeprang and H. G. Kjaergaard, *Phys. Chem. Chem. Phys.*, 2013, **15**, 10194-10206.
11. P. Schuster, G. Zundel and C. Sandorfy, *The Hydrogen Bond. Recent Developments in Theory and Experiments*, North-Holland Publishing Co., Amsterdam, 1976.
12. M. A. Boyer, O. Marsalek, J. P. Heindel, T. E. Markland, A. B. McCoy and S. S. Xantheas, *J. Phys. Chem. Lett.*, 2019, **10**, 918-924.
13. R. J. Thatcher, D. G. Johnson, J. M. Slattery and R. E. Douthwaite, *Chem. Eur. J.*, 2016, **22**, 3414-3421.
14. E. Gougoula, C. Medcraft, I. Alkorta, N. R. Walker and A. C. Legon, *J. Chem. Phys.*, 2019, **150**, 084307.
15. I. Alkorta and A. Legon, *Molecules*, 2018, **23**, 2250.
16. S. J. Grabowski, *Struct. Chem.*, 2019, **30**, 1141-1152.
17. S. Grabowski, *Molecules*, 2018, **23**, 1183.
18. S. Scheiner, *Phys. Chem. Chem. Phys.*, 2024, **26**, 27382-27394.
19. A. Franconetti and A. Frontera, *Chem. Eur. J.*, 2019, **25**, 6007-6013.
20. Z. Latajka and S. Scheiner, *J. Chem. Phys.*, 1984, **81**, 407-409.
21. J. S. Murray and P. Politzer, *J. Mol. Model.*, 2019, **25**, 101.
22. T. Clark, J. S. Murray and P. Politzer, *Phys. Chem. Chem. Phys.*, 2018, **20**, 30076-30082.
23. K. E. Riley and K.-A. Tran, *Faraday Disc.*, 2017, **203**, 47-60.
24. W. Zierkiewicz, M. Michalczyk, R. Wysokiński and S. Scheiner, *Molecules*, 2019, **24**, 376.
25. W. Dong, Y. Wang, J. Cheng, X. Yang and Q. Li, *Mol. Phys.*, 2019, **117**, 251-259.
26. G. Orlova and S. Scheiner, *J. Phys. Chem. A*, 1998, **102**, 4813-4818.
27. M. Esrafili and P. Mousavian, *Molecules*, 2018, **23**, 2642.
28. S. Scheiner and U. Adhikari, *J. Phys. Chem. A*, 2011, **115**, 11101-11110.
29. J. E. Del Bene, I. Alkorta and J. Elguero, *Chem. Phys. Lett.*, 2016, **655–656**, 115-119.
30. S. A. Southern and D. L. Bryce, *J. Phys. Chem. A*, 2015, **119**, 11891-11899.
31. V. d. P. N. Nziko and S. Scheiner, *Phys. Chem. Chem. Phys.*, 2016, **18**, 3581-3590.
32. M. Liu, Q. Li and S. Scheiner, *Phys. Chem. Chem. Phys.*, 2017, **19**, 5550-5559.
33. S. Scheiner, *J. Phys. Chem. A*, 2020, **124**, 7290-7299.
34. G. Cavallo, P. Metrangolo, R. Milani, T. Pilati, A. Priimagi, G. Resnati and G. Terraneo, *Chem. Rev.*, 2016, **116**, 2478-2601.
35. E. Corradi, S. V. Meille, M. T. Messina, P. Metrangolo and G. Resnati, *Tetrahedron Lett.*, 1999, **40**, 7519-7523.
36. J. Viger-Gravel, S. Leclerc, I. Korobkov and D. L. Bryce, *CrystEngComm*, 2013, **15**, 3168-3177.
37. R. S. Drago and D. Bafus, *J. Phys. Chem.*, 1961, **65**, 1066-1067.

38. D. W. Larsen and A. L. Allred, *J. Am. Chem. Soc.*, 1965, **87**, 1219-1226.
39. I. I. Schuster and J. D. Roberts, *J. Org. Chem.*, 1979, **44**, 2658-2662.
40. H. G. Loehr, A. Engel, H. P. Josel, F. Voegtle, W. Schuh and H. Puff, *J. Org. Chem.*, 1984, **49**, 1621-1627.
41. C. Laurence, M. Queignec-Cabanetos and B. Wojtkowiak, *Can. J. Chem.*, 1983, **61**, 135-138.
42. K. Gao and N. S. Goroff, *J. Am. Chem. Soc.*, 2000, **122**, 9320-9321.
43. J. Viger-Gravel, J. E. Meyer, I. Korobkov and D. L. Bryce, *CrystEngComm*, 2014, **16**, 7285-7297.
44. I. Alkorta, J. Elguero, M. Yáñez, O. Mó and M. M. Montero-Campillo, *Molecules*, 2019, **24**, 4399.
45. Y.-P. Chang, T. Tang, J. R. Jagannathan, N. Hirbawi, S. Sun, J. Brown and A. K. Franz, *Org. Lett.*, 2020, **22**, 6647-6652.
46. P. C. Vioglio, M. R. Chierotti and R. Gobetto, *CrystEngComm*, 2016, **18**, 9173-9184.
47. W. N. Moss and N. S. Goroff, *J. Org. Chem.*, 2005, **70**, 802-808.
48. S. Yu, J. M. Rautiainen, P. Kumar, L. Gentiluomo, J. S. Ward, K. Rissanen and R. Puttreddy, *Advanced Science*, 2023, **n/a**, 2307208.
49. P. D. Rege, O. L. Malkina and N. S. Goroff, *J. Am. Chem. Soc.*, 2002, **124**, 370-371.
50. R. Puttreddy, J. M. Rautiainen, S. Yu and K. Rissanen, *Angew. Chem. Int. Ed.*, 2023, **62**, e202307372.
51. J. Jaźwiński, in *Annual Reports on NMR Spectroscopy*, ed. G. A. Webb, Academic Press2021, vol. 104, pp. 1-73.
52. C. B. Aakeröy, S. Panikkattu, P. D. Chopade and J. Desper, *CrystEngComm*, 2013, **15**, 3125-3136.
53. C. B. Aakeröy, M. Fasulo, N. Schultheiss, J. Desper and C. Moore, *J. Am. Chem. Soc.*, 2007, **129**, 13772-13773.
54. L. P. Wolters and F. M. Bickelhaupt, *ChemistryOpen*, 2012, **1**, 96-105.
55. L. Posavec, V. Nemec, V. Stilinović and D. Cinčić, *Cryst. Growth Des.*, 2021, **21**, 6044-6050.
56. F. F. Awwadi, D. Taher, S. F. Haddad and M. M. Turnbull, *Cryst. Growth Des.*, 2014, **14**, 1961-1971.
57. F. Zapata, A. Caballero, P. Molina, I. Alkorta and J. Elguero, *J. Org. Chem.*, 2014, **79**, 6959-6969.
58. S. Li, T. Xu, T. van Mourik, H. Früchtl, S. R. Kirk and S. Jenkins, *Molecules*, 2019, **24**, 2875.
59. B. Nepal and S. Scheiner, *Chem. Eur. J.*, 2015, **21**, 13330-13335.
60. D. W. Larsen and A. L. Allred, *J. Phys. Chem.*, 1965, **69**, 2400-2401.
61. R. D. Green and J. S. Martin, *J. Am. Chem. Soc.*, 1968, **90**, 3659-3668.
62. D. E. Martire, J. P. Sheridan, J. W. King and S. E. O'Donnell, *J. Am. Chem. Soc.*, 1976, **98**, 3101-3106.
63. S. J. Grabowski, *Phys. Chem. Chem. Phys.*, 2013, **15**, 7249-7259.
64. E. Adeniyi, O. Grounds, Z. Stephens, M. Zeller and S. V. Rosokha, *Molecules*, 2022, **27**, 6124.
65. M. J. Frisch, G. W. Trucks, H. B. Schlegel, G. E. Scuseria, M. A. Robb, J. R. Cheeseman, G. Scalmani, V. Barone, G. A. Petersson, H. Nakatsuji, X. Li, M. Caricato, A. V. Marenich, J. Bloino, B. G. Janesko, R. Gomperts, B. Mennucci, H. P. Hratchian, J. V.

Ortiz, A. F. Izmaylov, J. L. Sonnenberg, D. Williams-Young, F. Ding, F. Lipparini, F. Egidi, J. Goings, B. Peng, A. Petrone, T. Henderson, D. Ranasinghe, V. G. Zakrzewski, J. Gao, N. Rega, G. Zheng, W. Liang, M. Hada, M. Ehara, K. Toyota, R. Fukuda, J. Hasegawa, M. Ishida, T. Nakajima, Y. Honda, O. Kitao, H. Nakai, T. Vreven, K. Throssell, J. A. Montgomery Jr., J. E. Peralta, F. Ogliaro, M. J. Bearpark, J. J. Heyd, E. N. Brothers, K. N. Kudin, V. N. Staroverov, T. A. Keith, R. Kobayashi, J. Normand, K. Raghavachari, A. P. Rendell, J. C. Burant, S. S. Iyengar, J. Tomasi, M. Cossi, J. M. Millam, M. Klene, C. Adamo, R. Cammi, J. W. Ochterski, R. L. Martin, K. Morokuma, O. Farkas, J. B. Foresman and D. J. Fox, Gaussian 16, Gaussian Inc., Wallingford, CT2016.

66. F. Weigend, *Phys. Chem. Chem. Phys.*, 2006, **8**, 1057-1065.
67. Y. Zhao and D. G. Truhlar, *Acc. Chem. Res.*, 2008, **41**, 157-167.
68. Y. Zhao and D. G. Truhlar, *Theor. Chem. Acc.*, 2008, **120**, 215-241.
69. G. Paytakov, T. Dinadayalane and J. Leszczynski, *J. Phys. Chem. A*, 2015, **119**, 1190-1200.
70. B. S. D. R. Vamhindi and A. Karton, *Chem. Phys.*, 2017, **493**, 12-19.
71. R. Podeszwa and K. Szalewicz, *J. Chem. Phys.*, 2012, **136**, 161102.
72. S. Karthikeyan, V. Ramanathan and B. K. Mishra, *J. Phys. Chem. A*, 2013, **117**, 6687-6694.
73. M. Majumder, B. K. Mishra and N. Sathyamurthy, *Chem. Phys.*, 2013, **557**, 59-65.
74. M. A. Vincent and I. H. Hillier, *Phys. Chem. Chem. Phys.*, 2011, **13**, 4388-4392.
75. A. D. Boese, *ChemPhysChem.*, 2015, **16**, 978-985.
76. M. Walker, A. J. A. Harvey, A. Sen and C. E. H. Dessent, *J. Phys. Chem. A*, 2013, **117**, 12590-12600.
77. L. F. Molnar, X. He, B. Wang and K. M. Merz, *J. Chem. Phys.*, 2009, **131**, 065102.
78. S. F. Boys and F. Bernardi, *Mol. Phys.*, 1970, **19**, 553-566.
79. T. Lu and F. Chen, *J. Mol. Graph. Model.*, 2012, **38**, 314-323.
80. T. Lu and F. Chen, *J. Comput. Chem.*, 2012, **33**, 580-592.
81. T. A. Keith, TK Gristmill Software, Overland Park KS2013.
82. R. F. W. Bader, *J. Phys. Chem. A*, 1998, **102**, 7314-7323.
83. P. L. A. Popelier, *Atoms in Molecules. An Introduction*, Prentice Hall, Harlow, UK, 2000.
84. R. Ditchfield, *Mol. Phys.*, 1974, **27**, 789-807.
85. R. Ditchfield, *Chem. Phys. Lett.*, 1976, **40**, 53-56.
86. Y. Gu, T. Kar and S. Scheiner, *J. Am. Chem. Soc.*, 1999, **121**, 9411-9422.
87. S. Scheiner, S. J. Grabowski and T. Kar, *J. Phys. Chem. A*, 2001, **105**, 10607-10612.
88. S. Scheiner and T. Kar, *J. Phys. Chem. A*, 2002, **106**, 1784-1789.
89. E. R. Johnson, S. Keinan, P. Mori-Sanchez, J. Contreras-Garcia, A. J. Cohen and W. Yang, *J. Am. Chem. Soc.*, 2010, **132**, 6498-6506.
90. J. F. Bertrán and M. Rodríguez, *Org. Mag. Res.*, 1980, **14**, 244-246.
91. J. F. Bertrán and M. Rodríguez, *Org. Mag. Res.*, 1979, **12**, 92-94.
92. B. Watson, O. Grounds, W. Borley and S. V. Rosokha, *Phys. Chem. Chem. Phys.*, 2018, **20**, 21999-22007.
93. S. V. Rosokha, I. S. Neretin, T. Y. Rosokha, J. Hecht and J. K. Kochi, *Heteroatom Chem.*, 2006, **17**, 449-459.

Table 1. V_{max} (kcal/mol) on H and X atoms, C-H bondlength, frequency and intensity of C-H stretching mode, and shielding of H and C atoms of CX_3H monomers.

	CF_3H	CCl_3H	CBr_3H	CI_3H
V_{max}(H), kcal/mol	34.6	33.3	33.0	29.9
V_{max}(X), kcal/mol	-	13.3	19.1	25.9
r(CH), Å	1.0895	1.0818	1.0806	1.0810
ν(CH), cm^{-1}	3175.6	3201.8	3213.4	3210.5
I(CH), km/mol	30.0	0.9	6.8	11.7
σ(H), ppm	25.78	24.82	24.65	25.28
σ(C), ppm	63.36	85.89	91.28	125.72

Table 2. Intermolecular distances (R, Å) and angles (α, degs) in HB and XB dyads.

	R		α	
	HB	XB	HB	XB
F^-				
CF_3H	1.399	-	180.0	-
CCl_3H	pT	2.182	pT[a]	176.9
CBr_3H	pT	2.111	pT	177.2
CI_3H	pT	2.130	pT	177.0
Cl^-				
CF_3H	2.218	-	179.9	-
CCl_3H	2.066	2.917	179.8	175.5
CBr_3H	2.015	2.791	179.9	176.5
CI_3H	1.988	2.727	179.8	176.6
Br^-				
CF_3H	2.443	-	179.7	-
CCl_3H	2.301	3.149	180.0	174.9
CBr_3H	2.254	3.021	179.8	176.1
CI_3H	2.222	2.929	179.1	176.5
I^-				
CF_3H	2.726	-	179.9	-
CCl_3H	2.573	3.421	179.7	173.9
CBr_3H	2.519	3.302	179.7	175.6
CI_3H	2.481	3.164	178.6	176.4
NH_3				
CF_3H	2.307	-	179.1	-
CCl_3H	2.272	2.999	133.4	178.9
CBr_3H	2.242	2.983	137.5	179.5
CI_3H	2.194	2.979	149.3	178.8
NCH				
CF_3H	2.418	-	178.0	-
CCl_3H	2.421	3.138	131.2	179.7
CBr_3H	2.402	3.132	134.7	177.8
CI_3H	2.419	3.127	137.9	178.1

[a]proton transfer

Table 3. Interaction energies of dyads, and the effect of dimerization on the CH bond length, frequency and intensity of the C-H stretching vibration within the CX_3H subunits

	$-E_{int}$, kcal/mol		Δr_{CH}, Å		$\Delta\nu_{CH}$, cm^{-1}		I/I_o	
	HB	XB	HB	XB	HB	XB	HB	XB
F^-								
CF_3H	36.86	-	0.0908	X	-1169.5	-	32.9	X
CCl_3H	pT	20.86	pT	0.0017	pT	-35.0	pT	6.1
CBr_3H	pT	33.82	pT	0.0025	pT	-34.8	pT	0.3
CI_3H	pT	51.16	pT	0.0041	pT	-46.8	pT	0.3
Cl^-								
CF_3H	17.34	-	0.0109	-	-173.4	-	9.0	X
CCl_3H	18.95	9.65	0.0311	0.0007	-492.4	-21.4	1485.6	1.6
CBr_3H	20.18	16.47	0.0382	0.0010	-613.8	-17.7	245.9	0.4
CI_3H	20.50	28.10	0.0414	0.0029	-651.3	-35.5	156.1	0.7
Br^-								
CF_3H	14.54	-	0.0066	-	-96.8	-	5.8	X
CCl_3H	15.56	7.58	0.0208	0.0006	-312.4	-19.2	1105.4	1.0
CBr_3H	16.50	13.22	0.0251	0.0006	-394.4	-14.9	189.8	0.4
CI_3H	16.86	23.39	0.0272	0.0026	-436.1	-33.2	124.7	0.9
I^-								
CF_3H	12.00	-	0.0037	-	-48.9	-	3.4	X
CCl_3H	12.71	5.74	0.0146	0.0005	-209.1	-17.0	843.2	0.6
CBr_3H	13.48	10.43	0.0177	0.0004	-258.4	-11.9	151.5	0.5
CI_3H	13.95	19.42	0.0192	0.0024	-287.1	-31.4	102.0	1.2
NH_3								
CF_3H	4.39	-	0.0008	-	-2.8	-	0.4	X
CCl_3H	5.48	2.28	0.0021	0.0005	-17.8	-13.0	86.8	0.3
CBr_3H	5.77	3.53	0.0029	0.0000	-26.7	-2.3	18.6	1.6
CI_3H	5.67	5.67	0.0043	0.0004	-56.5	-8.0	18.1	0.7
NCH								
CF_3H	2.82	-	-0.0016	-	30.3	-	0.0	X
CCl_3H	3.41	0.99	0.0012	0.0004	0.2	-7.0	14.9	0.6
CBr_3H	3.58	1.67	0.0012	-0.0002	-3.1	-1.6	4.1	0.8
CI_3H	3.63	2.82	0.0016	0.0001	-13.5	-4.9	3.1	0.8

Table 4. Changes in shielding (ppm) of H and C atoms of haloform caused by complexation.

	H		C	
	HB	XB	HB	XB
F^-				
CF_3H	-10.6	-	-16.6	-
CCl_3H	pT	0.8	pT	-4.8
CBr_3H	pT	1.0	pT	-11.4
CI_3H	pT	0.9	pT	-21.5
Cl^-				
CF_3H	-5.2	-	-4.8	-
CCl_3H	-6.5	0.5	-12.3	-0.1
CBr_3H	-6.6	0.8	-20.6	-2.0
CI_3H	-6.4	0.9	-32.8	-11.4
Br^-				
CF_3H	-4.5	-	-3.6	-
CCl_3H	-5.2	0.4	-10.1	0.4
CBr_3H	-5.2	0.7	-17.3	-0.6
CI_3H	-4.7	0.9	-28.4	-8.9
I^-				
CF_3H	-3.8	-	-2.6	-
CCl_3H	-4.2	0.4	-8.5	1.0
CBr_3H	-4.0	0.6	-14.7	0.9
CI_3H	-3.3	0.9	-24.8	-6.7
NH_3				
CF_3H	-2.2	-	-1.6	-
CCl_3H	-1.8	0.2	-4.4	0.7
CBr_3H	-1.8	0.3	-6.8	1.7
CI_3H	-2.1	0.5	-10.0	2.5
NCH				
CF_3H	-0.4	-	-0.8	-
CCl_3H	-0.6	0.1	-2.8	0.4
CBr_3H	-0.5	0.2	-4.2	1.1
CI_3H	-0.4	0.3	-6.3	2.0

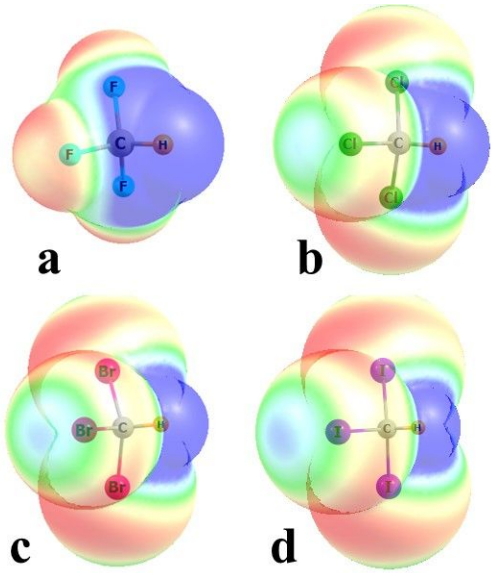

Fig 1. Molecular electrostatic potential of a) CF_3H, b) CCl_3H, c) CBr_3H, and d) CI_3H, on a surface corresponding to 1.5x vdW radius. Blue color represents +19 kcal/mol, while -6 kcal/mol is indicated by the red color.

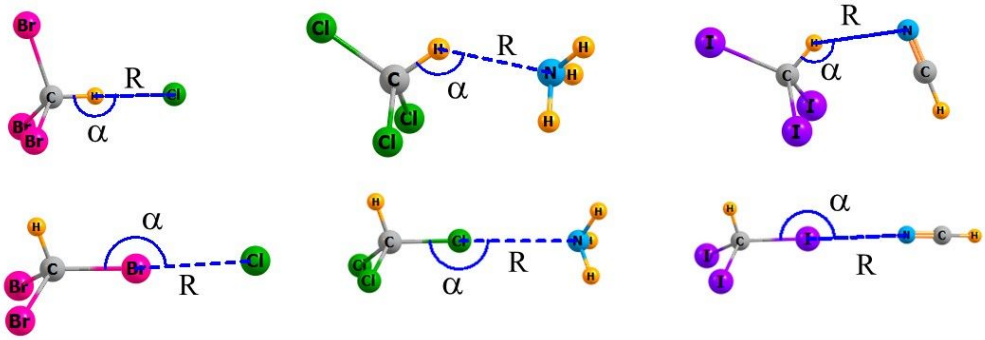

Fig 2. Geometries of several representative dyads, which define the intermolecular distance R and the HB/XB angle α.

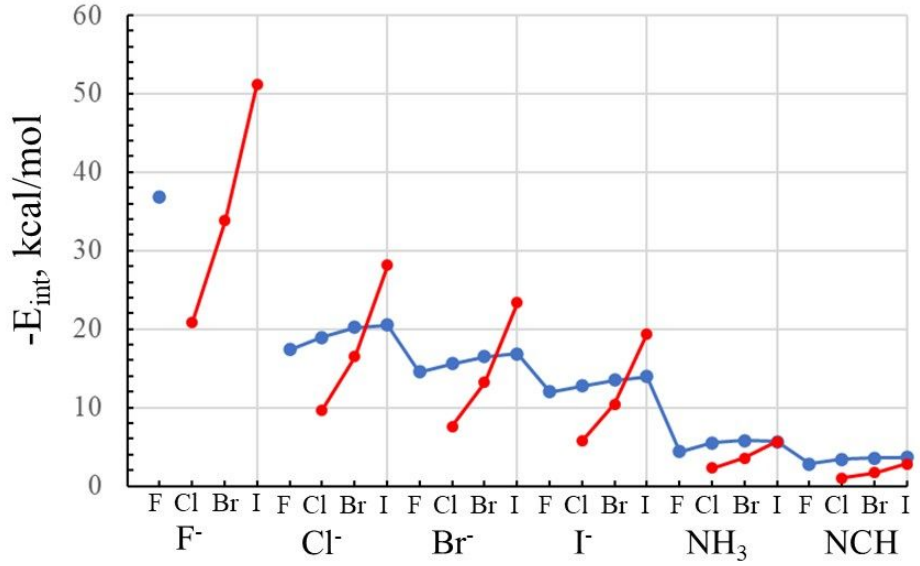

Fig 3. Dependence of interaction energy of HB (blue curve) and XB (red curve) for dyads containing haloform and indicated nucleophile.

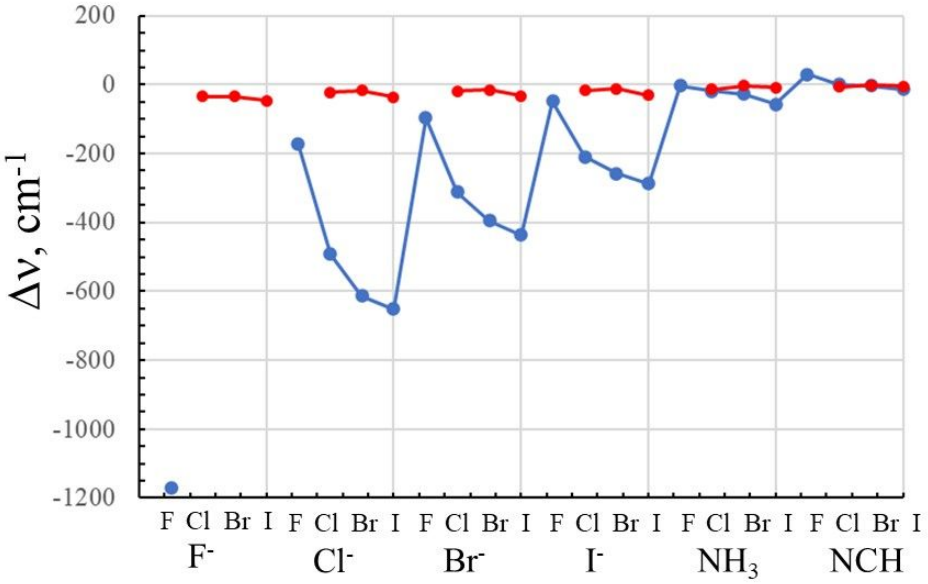

Fig 4. Shift of CH (blue curve) and XH (red curve) stretching frequency of each haloform caused by complexation with the indicated nucleophile.

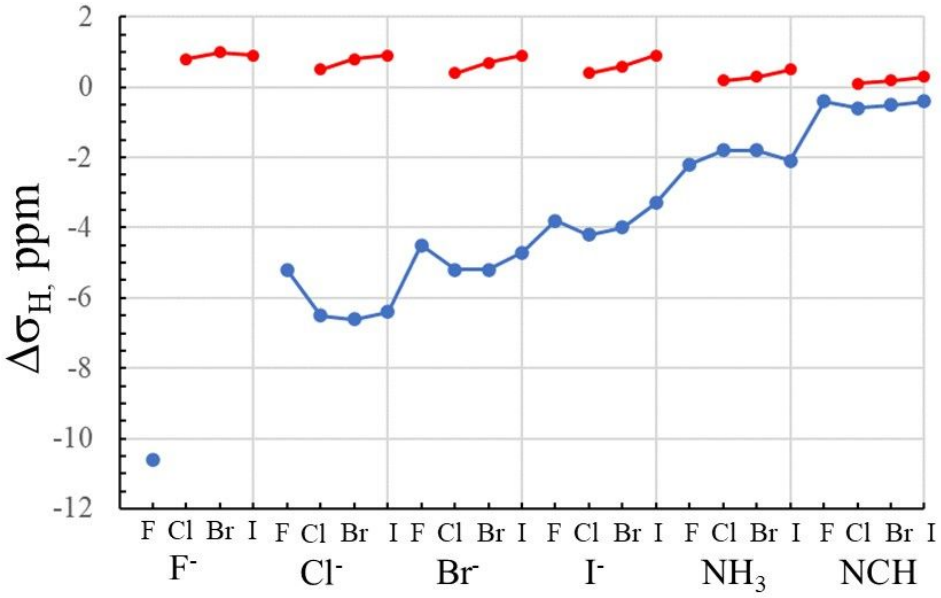

Fig 5. Change of shielding of haloform H nucleus caused by formation of HB (blue curve) and XB (red curve).

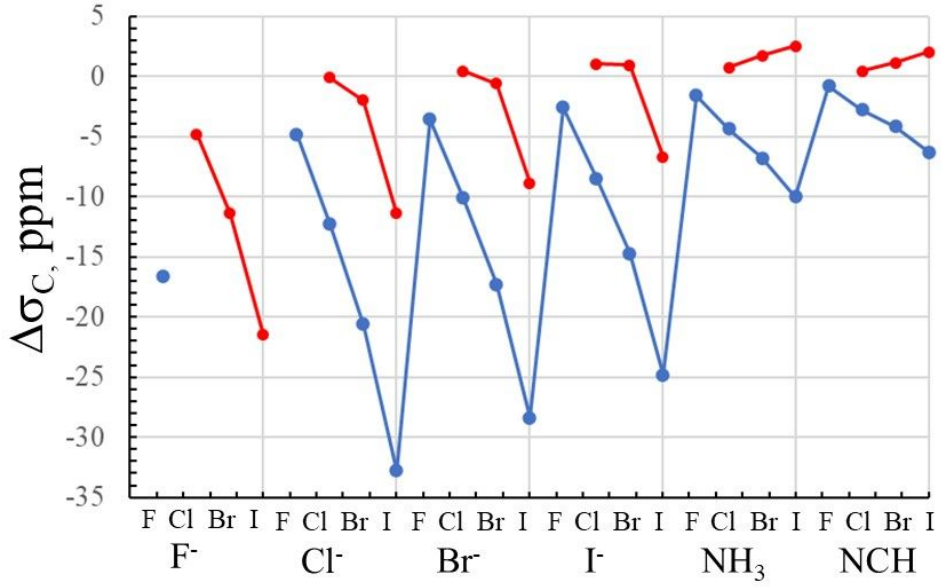

Fig 6. Change of shielding of haloform C nucleus caused by formation of HB (blue curve) and XB (red curve).

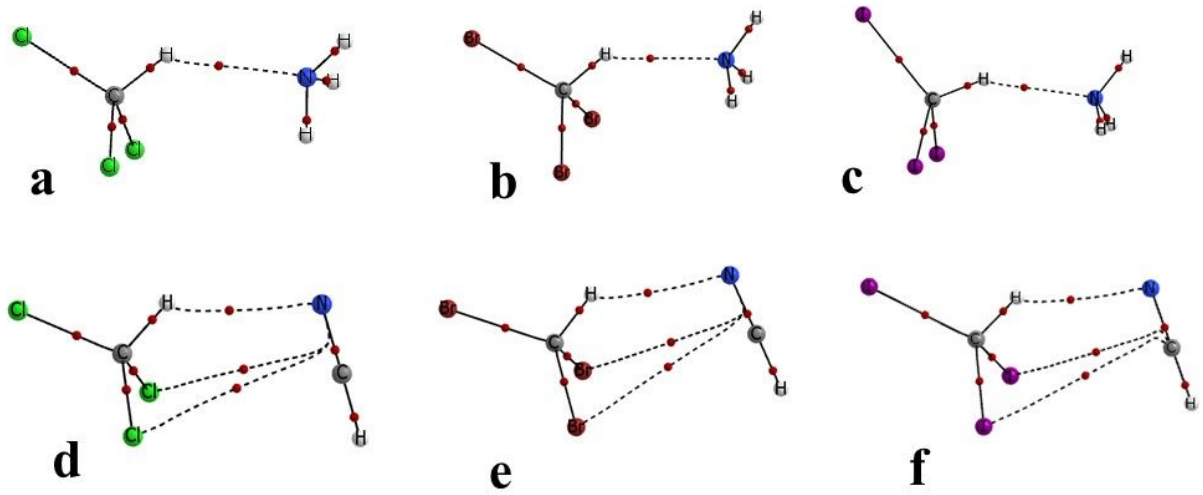

Fig 7. AIM diagrams of a) $CCl_3H\cdot\cdot NH_3$, b) $CBr_3H\cdot\cdot NH_3$, c) $CI_3H\cdot\cdot NH_3$, d) $CCl_3H\cdot\cdot NCH$, e) $CBr_3H\cdot\cdot NCH$, f) $CI_3H\cdot\cdot NCH$.

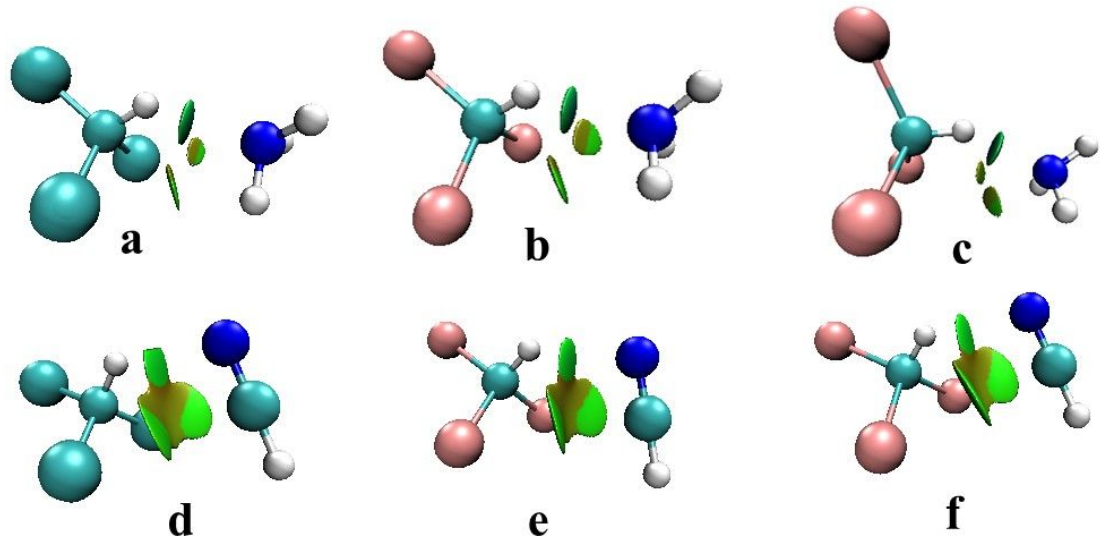

Fig 8. NCI diagrams of a) $CCl_3H\cdot\cdot NH_3$, b) $CBr_3H\cdot\cdot NH_3$, c) $CI_3H\cdot\cdot NH_3$, d) $CCl_3H\cdot\cdot NCH$, e) $CBr_3H\cdot\cdot NCH$, f) $CI_3H\cdot\cdot NCH$. Green regions signify weak attractive bonding.

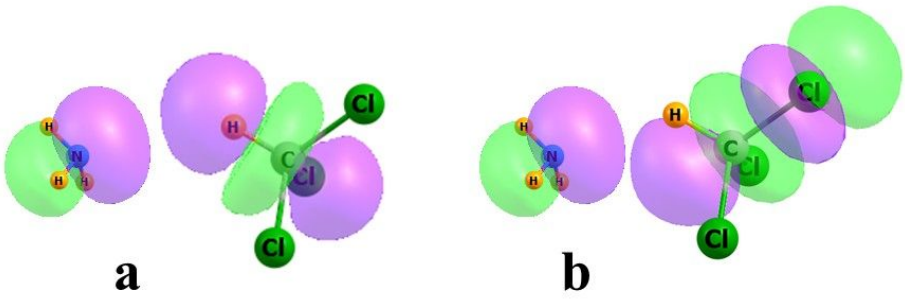

Fig 9. Disposition of NH_3 lone pair orbital in relation to a) σ*(CH) and b) σ*(CCl) antibonding orbital of CCl_3H.

Data are available from the author upon request.